Impact of electrostatic fields in layered crystalline BCS superconductors

Luca Chirolli [1,2] Tommaso Cea,[3,4] and Francesco Giazotto [2]
[1]*Department of Physics, University of California, Berkeley, California 94720, USA*
[2]*NEST, Istituto Nanoscienze-CNR and Scuola Normale Superiore, I-56127 Pisa, Italy*
[3]*Instituto de Ciencia de Materiales de Madrid, CSIC, ES-28049 Cantoblanco Madrid, Spain*
[4]*Imdea Nanoscience, ES-28049 Cantoblanco Madrid, Spain*

(Received 29 December 2020; revised 16 March 2021; accepted 16 April 2021; published 21 May 2021)

Motivated by recent experiments reporting the suppression of the critical current in superconducting Dayem bridges by the application of strong electrostatic fields, in this paper we study the impact on the superconducting gap of charge redistribution in response to an applied electric field in thin crystalline metals. By numerically solving the BCS gap equation and the Poisson equation in a fully self-consistent way, we find that the gap becomes sensitive to the applied electric field when the size of the gap becomes an order of magnitude larger than the average level spacing of the spectrum in the normal state. In this case, the gap shows sudden rises and falls that are compatible with surface modifications of the local density of states. The effect is washed out by increasing the pairing strength toward the weak-to-moderate coupling limit or by introduction of a weak smearing in the density of states that effectively mimics a thicker sample and a weakly disordered system.

DOI: 10.1103/PhysRevResearch.3.023135

I. INTRODUCTION

A thorough understanding of the impact of electrostatic fields on superconductivity is of great relevance from a fundamental point of view, as it may represent an easy-access active knob to control fundamental quantum states of matter and open the way to a number of technological applications. Electrostatic fields have been successfully employed in systems where the carrier density is low, such as thin crystalline films [1–4], band insulators [5–7], interfaces [8], semiconducting, and low-density two-dimensional materials [9–12], or to tune the proximity effect [13–15]. In most cases, the electrostatic field controls the carrier density by shifting the active bands of the material. A low electronic density yields poor screening and, in sufficiently thin structures, the electric field fully penetrates. In these cases, the electrostatic force squeezes the electron gas and effectively reduces the thickness of the material by adding the electrostatic potential to the confining potential. The superconducting properties in thin samples are known to be strongly thickness dependent. Average gap and critical temperature have been studied in nanowires [16–19], nanofilms [20–24], and nanograins [25–30]. Effects of the confinement typically appear as shape resonances, critical field [17] and critical current oscillations [18], and strong dependence of the longitudinal coherence length on the thickness [19], that all arise when progressively depleting subbands. In contrast, metals characterized by a high carrier density screen very well the electrostatic field within a few angstroms from the surface [31–34] and the residual skin contribution is typically negligible at the level of carrier density and density of states (DoS). Superconductors realized in diffusive metals are typically hardly affected by electrostatic fields.

Recently, a series of experiments conducted on metallic superconducting Dayem nanobridges have shown that a strong electric field, generated by a high voltage applied on a side gate, is able to switch the critical current I_c of the Dayem bridge off in a reversible ambipolar way [35–39]. Although a certain material dependence is observed, with a pronounced effect in Nb, Va, Ti, the effect seams to be relatively general, as it occurs in Al-Cu-Al proximity Josephson junctions [40] and in Al Dayem bridges [41]. Possible leakage currents and related overheating effects [42–44] have been minimized by constructing suspended nanobridges [45]. Measurement of the switching current distribution shows the presence of very strong gate-induced phase fluctuations [46]. Theoretical attempts to explain the origin of the observed field effect suggested a surface orbital polarization [41,47,48] and a possible Schwinger effect [49]. These findings are yet to be understood in the usual framework of the BCS theory and represent a challenge from a fundamental point of view, whose solution may reveal great technological interest. Although the observed phenomenology involves diffusive polycrystalline metals, it offers the opportunity to study the impact of an electric field in systems at the boundary between low-density crystalline materials and diffusive metals.

In this paper, we address the problem of gate-controlling superconductivity in thin metallic clean systems, consisting of a crystal composed by N layers and characterized by a large carrier density, large DoS at the Fermi level, albeit still with a well-defined notion of discreteness. Rather then studying

the effect of variation of the carrier density, we focus on the impact of a redistribution of charge in response to an applied electric field by choosing an antisymmetric profile of the potential in a capacitorlike configuration. In a particle-hole symmetric spectrum, this guarantees only the bipolar part of the effect is described, leaving aside global carrier density modifications. We numerically solve the fully self-consistent gap equation and Poisson electrostatic equation describing simultaneous condensation of a superconducting gap and screening of the applied field within the BCS theory. The screening length is only slightly increased from its metallic counterpart, in agreement with random-phase approximation results first described by Anderson [50] and Thouless [51], that predict a correction of order $(\Delta/E_F)^2$ [33], with Δ the superconducting gap and E_F the Fermi energy [52].

To enhance the responsiveness of the system, we choose as the basic system a tight-binding model in the cubic lattice that yields a particle-hole symmetric normal-state spectrum, but results are qualitatively confirmed with an in-plane triangular lattice. We find that for a small relative dielectric constant, relatively large system size, and strong superconducting pairing, the gap is essentially insensitive to the applied field. In turn, by reducing the pairing strength, we observe an increased sensitivity to the applied field, with the gap showing sudden rises and falls as the applied voltage is increased.

In agreement with previous studies on superconducting nanograins [25–30], the relevant quantity that controls the behavior of the system is the ratio between the average level spacing in the normal state and the gap. Besides the coherence length and the Fermi wavelength, a third length scale can be defined, as the size of the system for which the average level spacing is equal to the gap [30]. We find that when the level spacing is about one order of magnitude smaller than the gap, a condition typical of large nanograins, the system becomes sensitive to DoS modification induced by the screened potential. The latter adds to the confining potential and plays the role of a layer chemical potential. Although the exponentially decaying profile significantly modifies only the outermost few layers, our results show that it can result in sizable bulk effects. For a perfectly clean crystalline structure, the entire DoS spanning the whole bandwidth is necessary to account for the observed behavior. In turn, the introduction of a weak energy smearing in the DoS washes out the effect and the gap follows mainly the DoS at the Fermi level. Indeed, a weak smearing emulates the effect of weak disorder and an increased thickness, as it eliminates accidental degeneracies, smoothens the DoS profile, and cuts van Hove singularities.

Our results apply to clean large grains and granular systems in the weak-coupling limit and show how an evolution from a clean to a weakly disordered system effectively takes place. These results are expected to be significant for granular systems of layered materials and thin crystalline metals and predicts a certain degree of control of superconductivity through an applied electrostatic field.

II. MEAN-FIELD BCS WITH SCREENING

We consider a system composed by N layers, as depicted in Fig. 1, each described by a spin-degenerate microscopic tight-binding model. For simplicity, we assume a single orbital per unit cell, with nearest-neighbor hopping t, that results in a dispersion $\epsilon_{\mathbf{k}}$, with $\mathbf{k}$ in-plane momentum. Interlayer nearest-neighbor hopping is described by the same hopping t. Electrons interact via a purely local two-body attraction described by a Hubbard term with strength U that acts as a pairing interaction. In addition, we apply an external electric field $\mathbf{E}_g$ along the out-of-plane z direction via a side gate. The electric field is screened by the electron gas and the full electric field E_i^z can be introduced that is described via an electrostatic energy potential ϕ_i, such that $E_{i+1}^z = -(\phi_{i+1} - \phi_i)/ae$, with a the lattice constant and e the electric charge. The full Hamiltonian then reads

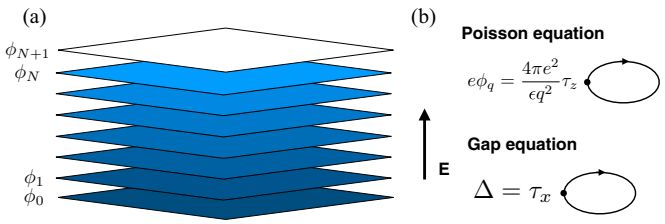

FIG. 1. (a) Schematics of the system composed by N layers. The electric field is applied along the out-of-plane direction and is modeled by fixing the electrostatic potential at the $i = 0$ and $i = N + 1$ layers. (b) Diagrammatic form of the Poisson equation and the gap equation.

$$H = \sum_{\mathbf{k},i,s}(\epsilon_{\mathbf{k}} - \phi_i)c^\dagger_{\mathbf{k},i,s}c_{\mathbf{k},i,s} - t\sum_{i,s}(c^\dagger_{\mathbf{k},i+1,s}c_{\mathbf{k},i,s} + \text{H.c.}) - \frac{U}{N_k}\sum_{\mathbf{k},\mathbf{k}',i} c^\dagger_{\mathbf{k},i,\uparrow}c^\dagger_{-\mathbf{k},i,\downarrow}c_{-\mathbf{k}',i,\downarrow}c_{\mathbf{k}',i,\uparrow} + V_C, \quad (1)$$

where V_C is the Coulomb interaction. The latter is crucial to correctly describe screening of the applied field. Its continuum form in Fourier transform is given by $V_C(\mathbf{q}, q_z) = 4\pi e^2/(\epsilon(q^2 + q_z^2))$, with ϵ the dielectric coupling constant. The momentum transfer $(\mathbf{q}, q_z)$ is restricted to nonzero value to account for the background positive charge. We separate the in-plane and out-of-plane Coulomb interactions by singling out the $\mathbf{q} = 0$, $q_z \neq 0$ term, so that the Coulomb interaction reads

$$V_C = \frac{1}{2}\int dz dz' n(z) V_{\text{eff}}(z - z')n(z'), \quad (2)$$

with $V_{\text{eff}}(z - z') = \frac{1}{L}\sum_{q_z\neq 0} e^{iq_z(z-z')}4\pi e^2/(\epsilon q_z^2)$, $n(z_i) = \sum_{\mathbf{k},s} c^\dagger_{\mathbf{k},i,s}c_{\mathbf{k},i,s}$, and we neglect the residual interaction. Standard decoupling of Eq. (2) gives rise to the Poisson equation. By noticing that q_z^2 is the eigenvalue of the Laplacian in 1D, we directly write a discrete version of the Poisson equation in 1D as

$$-\phi_{i+1} - \phi_{i-1} + 2\phi_i = \frac{4\pi e^2}{\epsilon a}[n_i - n_0], \quad (3)$$

which ensures charge conservation locally on each layer.

The rest of the Hamiltonian is decoupled in the Cooper channel at the mean-field level by defining a local layer dependent gap, $\Delta_i = -\frac{U}{N_k}\sum_{\mathbf{k}}\langle c_{-\mathbf{k},i,\downarrow}c_{\mathbf{k},i,\uparrow}\rangle$. The Bogoliubov–de

Gennes (BdG) tight-binding Hamiltonian is written as

$$H = \sum_{\mathbf{k},ij} h_{ij}(\mathbf{k}) c^{\dagger}_{\mathbf{k},i,s} c_{\mathbf{k},j,s} + \Delta_i c^{\dagger}_{\mathbf{k},i,\uparrow} c^{\dagger}_{-\mathbf{k},i,\downarrow} + \text{H.c.}, \quad (4)$$

with $h_{ij}(\mathbf{k}) = [\epsilon_{\mathbf{k}} - \phi_i]\delta_{ij} - t(\delta_{i+1,j} + \delta_{i,j+1})$ and the chemical potential has been absorbed in the dispersion. The gap and the electron density are then written as

$$n_i = \frac{2}{N_k} \sum_{\mathbf{k}} v_i^2(\mathbf{k}), \quad \Delta_i = \frac{U}{N_k} \sum_{\mathbf{k}} u_i(\mathbf{k}) v_i(\mathbf{k}). \quad (5)$$

where the $u_i(\mathbf{k})$ and $v_i(\mathbf{k})$ are the particle and hole parts of the eigenvectors at layer i of the BdG Hamiltonian Eq. (4) and N_k is the number of $\mathbf{k}$ points in the Brillouin zone (BZ).

The equation for the gap and the density Eqs. (5) are solved iteratively together with the Poisson Eq. (3). For simplicity, we assume to insert the layered system in a capacitorlike structure that fixes the value of the gate voltage to be opposite on the two sides of the system. A uniform gap $\Delta^{(0)}$ and a linear potential $\phi_i^{(0)} = (2i/N - 1)\phi_g$ are assigned at the first step and the charge density and the gap are recursively updated. The potential ϕ_i is obtained via inversion of the Poisson Eq. (3) and by imposing a fixed boundary condition at the two most external layers $\phi_0 = -\phi_{N+1} = \phi_g$. The mean density n_0 is kept fixed at half filling and the chemical potential is updated to keep the half-filling condition at every step. Convergence is achieved within a threshold error smaller than 10^{-5} of a chi-squared error function for the three quantities n_i, Δ_i, ϕ_i. By increasing the gate in a discretized way, convergence speed highly increases, using as guesses for the gap, density, and potential those self-consistently obtained at a smaller value of the gate potential.

III. DENSITY OF STATES AND SCREENING

We assume the in-plane system to be described by a square lattice, so the dispersion reads

$$\epsilon_{\mathbf{k}} = -2t[\cos(k_x) + \cos(k_y)]. \quad (6)$$

At half filling, the chemical potential is $\mu = 0$. For a structure composed by a few layers, some concerns may arise from the half-filling van Hove singularity that characterizes the one-layer DoS. Strictly speaking, if N is odd, a smeared van Hove singularity still appears at half filling, whereas for N even, it is shifted at positive and negative energies by interlayer tunneling. To avoid peaks in the DoS at the Fermi level, we always choose an even number of layers.

We measure the strength of the Hubbard attraction U in units of the hopping energy t and group the lattice spacing a and the dielectric constant ϵ in the energy scale $e^2/(a\epsilon)$. Setting $a = 1$ Å, we define our Rydberg as $\text{Ry} = e^2/(\epsilon_0 a) = 18.05\,\text{eV} \equiv 18.05\,t$. This way, the only free parameters in the system are the number of layers N, the attraction strength U, the number $N_k = N_x N_y$ of $\mathbf{k}$ points in the BZ, and the relative dielectric constant ϵ_r. The smaller the dielectric constant ϵ_r, the stronger the screening.

In Fig. 2(a), we show a histogram of the multiplicity of the eigenvalues of a $N_x = N_y = 100$ grid in momentum space, for a system constituted by $N = 20$ layers. The histogram tends to the typical DoS of a 3D cubic lattice once a smearing in energy is assumed. Deviations due to finite-size effects both in plane and out of plane are evident and $N = 20$ peaks reminiscent of the original van Hove singularities are still present.

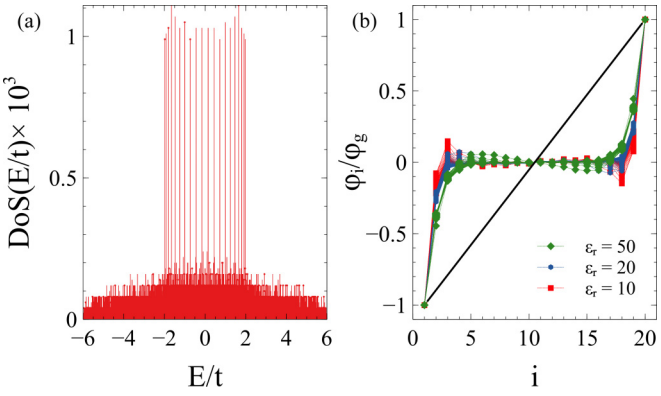

FIG. 2. (a) Histogram of the eigenvalues multiplicity (total density of states) in absence of applied gate. Width of the histogram bin $w/t = 2 \times 10^{-5}$. (b) Profile of the self-consistent potential for different values of the relative dielectric constant $\epsilon_r = 10, 20, 50$.

In Fig. 2(b), we show the self-consistent potential normalized to its maximum strength for values of the applied gate $0 < \phi_g < 5t$, for three different values of the relative dielectric constant $\epsilon_r = 10, 20, 50$. The field is screened very well by the metal and an overall exponential decay is recognized. In addition, oscillations of the charge on the scale of the screening length are present, indicating a local increase/decrease of the layer chemical potential ϕ_i in the bulk of the slab. The charge distribution screens the external field via charge accumulation at the outermost layers. The latter overshoots the one necessary to screen the field and a series of alternating electric dipoles on the scale of the screening lengths are generated to compensate local overshooting.

IV. SIMULATIONS

We now present the results of full numerical calculations. As pointed out in Sec. I, we expect no effect of the applied gate for a large system, characterized by strong screening and a relatively strong pairing, within the weak coupling limit. We confirm this expectation for a system composed by $N = 30$ layers, pairing strength $U = t$, relative dielectric constant $\epsilon_r = 10$, and $N_x = N_y = 100$ points in momentum space. The results of the simulations are shown in Fig. 3. The self-consistent gap and potential are shown in Figs. 3(a) and 3(c), respectively. The gap is mostly uniform through the slab for all values of the applied electric field. Small oscillations on the scale of the lattice constant appear on top of the average value. For strong fields, the gap in the outermost layer approaches zero at $\phi_g = 24\,t$. This arises because of complete charge saturation (depletion) in the outermost layer [shown in Fig. 3(d)] and the absence of available particle (hole) states locally suppresses the gap.

A. Average gap varying N and ϵ_r

We now study the impact of the applied field on the gap for samples with different thicknesses $N = 30, 20, 10$ for $U = t$.

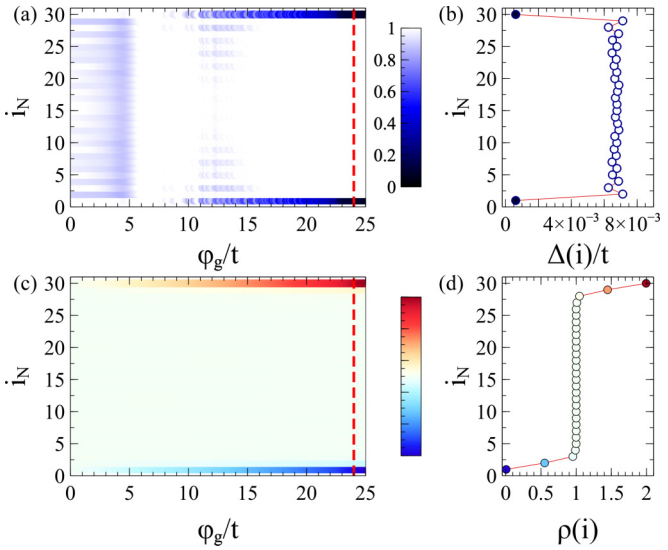

FIG. 3. Results of imulations for a strong pairing $U = t$ for a thick slab with $N = 30$. (a) Color plot of the local gap versus layer i_N and applied gate voltage ϕ_g. (b) Section of (a) at $\phi_g = 24\,t$ showing gap suppression in the outermost layers. (c) Value of the self-consistent charge density versus the layer i_N and the applied gate, showing charge depletion in the outermost layers. (d) Self-consistent charge density at $\phi_g = 24\,t$ showing full depletion at the outermost layer.

Results are shown in Fig. 4(a). The gap at zero applied gate voltage is not a monotonic function of the sample thickness and shows well-known quantum oscillations. The dependence on the applied gate is very smooth for $N = 20, 30$ and the gap shows robustness to the applied electric field. For $N = 10$, a sizable and smooth modulation of the gap is observed. We then fix the slab thickness to $N = 20$ and study the dependence of the layer-averaged gap $\Delta = \sum_i \Delta_i/N$ on the applied field for three values of the dielectric constant $\epsilon_r = 10, 20, 50$. Results are shown in Fig. 4(b). By increasing the value of ϵ_r, the gap shows an average smooth linear decrease with the applied gate that seems to saturate for higher values of

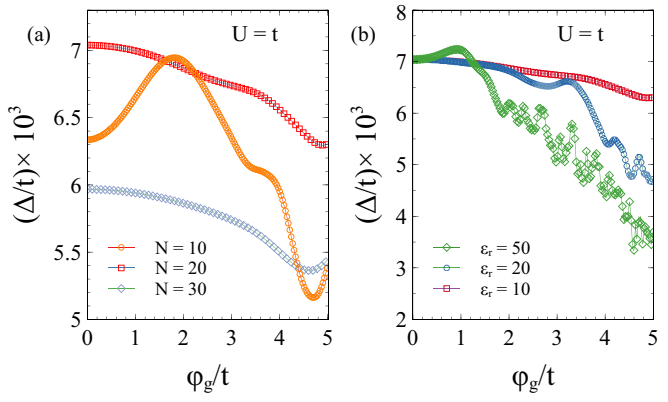

FIG. 4. Average gap Δ versus applied gate ϕ_g for $U = t$ varying (a) the number of layers $N = 10, 20, 30$ for $\epsilon_r = 10$ and (b) the relative dielectric constant $\epsilon_r = 10, 20, 50$ for $N = 20$. In-plane grid with $N_x = N_y = 100$.

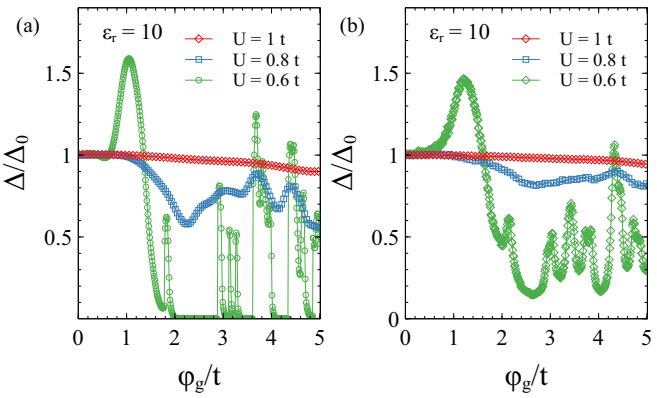

FIG. 5. (a) Normalized average gap versus applied gate voltage ϕ_g for different values of the pairing strength $U/t = 1, 0.8, 0.6$ for $\epsilon_r = 10$. (b) Gap calculated through Eq. (7) with the density of states $\nu(E)$ resulting from the self-consistent potential. Fixed parameters are $N = 20$ and $N_x = N_y = 100$. The values of the gap at zero voltage are $10^3\Delta_0/t = 7, 1.7, 0.22$ for $U/t = 1, 0.8, 0.6$, respectively.

ϵ_r, accompanied by fast irregular fluctuations on top of the linear decrease. The analysis is repeated for $U = 0.8\,t$ (results not shown). The average gap becomes more sensitive to the applied gate and strongly nonmonotonic rises and falls appear in correspondence with the smooth variations observed for $U = t$.

B. Average gap varying U

We now study the gap versus gate voltage curve varying U. The zero voltage gap clearly diminishes by decreasing U, so we normalize the curves with their zero voltage value $\Delta_0 = \Delta(\phi_g = 0)$. In Fig. 5(a), we show the results for $\epsilon_r = 10$. We see that by decreasing U, the effect of the gate becomes more and more pronounced. For $U = 0.6$ at $\phi_g \simeq 1.5\,t$, the gap drops to zero after a 50% increase and it stays zero apart from very sharp and sudden revivals. For the chosen value $\epsilon_r = 10$, the field penetrates only for a few layers. The weak modulation of the gap observed for large U is strongly amplified for smaller U. The analysis is repeated for $\epsilon_r = 50$ (results not shown) and the dependence on the gate voltage becomes more and more frustrated. We observe again that the small fluctuations appearing in the $U = t$ curves are strongly amplified for smaller U, suggesting a common DoS origin.

V. GAP FROM DOS

The analysis so far presented shows that a strong sensitivity to the gate appears when reducing the pairing strength U. We point out that in all simulations a smooth convergence of the self-consistent calculation is observed at every step, ruling out numerical instability. The BCS theory predicts that all properties of the superconducting gap are determined by the DoS of the system. The latter is typically assumed to be uniform over a large range of energies where the pairing is active and approximated with its value at the Fermi level. Clearly, this approximation fails if the DoS suffers strong modifications close to the Fermi level due to confinement,

as shown in Fig. 2(a), where the DoS at the Fermi level is ill-defined.

We then calculate the gap that results assuming the effect of the electric field comes solely by the screened potential ϕ_i. This is done by taking the self-consistently screened potential for every value of the applied gate voltage, calculating the DoS $\nu(E)$ in the normal phase, and self-consistently solving for the gap via the BCS gap equation

$$1 = U \int dE \frac{\nu(E)}{2\sqrt{E^2 + \Delta^2}} \tag{7}$$

by varying only U. The result for $\epsilon_r = 10$ is shown in Fig. 5(b): There is a good similarity between the curves shown in Fig. 5(a), showing how the unexpected behavior of the gap can be understood in terms of the full DoS and its readjustment with the screened potential. At the same time, we notice that the dependence on the field is smoother in the curve in Fig. 5(b): Although peaks and dips appear in the same ranges of gate voltage, a suppression of the gap is never observed. We ascribe these discrepancies to the fact that the finite size of the system sets a lower energy scale, that is given by the average level spacing of the spectrum. When the gap is much larger than the average level spacing, Eq. (7) is expected to be highly predictive. In the present case, we find a level spacing on the order of $3.5 \times 10^{-5} t$ in an energy window of 0.1 t around the Fermi energy. In turn, the gap at zero voltage is $\Delta_0/t = 2.2 \times 10^{-4}$ for $U = 0.6t$, so the gap is just an order of magnitude larger than the average level spacing. The situation is analogous to the case of superconducting nanograins [25–30] previously studied in literature.

It is clear that finite-size effects, in particular, the finite thickness, are at the origin of the observed sensitivity to the applied gate voltage for weaker value of U. Indeed, by reducing U, we reduce the ratio between the gap and the average level spacing. We can mimic a thicker system and a small amount of local disorder by smearing the DoS on a small energy window. We then convolve the DoS with a smoothening distribution of width $0.03t$ and obtain a coarse-grained DoS that effectively describes a metal characterized by moderate disorder and a thicker size. The result is shown in Fig. 6(a), where reminiscences of van Hove singularities are still visible. The DoS at the Fermi level is now a meaningful quantity and it is shown in Fig. 6(b) for three values of $\epsilon_r = 10, 20, 50$. We can then calculate the self-consistent gap via numerically integrating Eq. (7) for $U = 0.6t$ and $\epsilon_r = 50$. We see that the gap closely follows the behavior of the DoS at the Fermi level.

These results reliably predict a modulation of the gap in a clean metal via an external electric field that penetrates sufficiently in the system. At the origin is the finite size of the system that yields a finite average level spacing. When the latter is not much smaller than the gap, a condition that manifests when the pairing U is reduced, a high sensitivity on the applied gate voltage appears. The introduction of a weak smearing in the DoS does not qualitatively change the results that also apply to thin weakly disordered metal. Furthermore, comparison of Fig. 6(c) with Fig. 4(b) for $\epsilon_r = 50$ shows how the gap versus gate voltage for small U and moderate energy smearing is compatible with the gap dependence at large U without energy smearing. This shows how a strong gap can tolerate a slight readjustment of the density in response to an applied electric field.

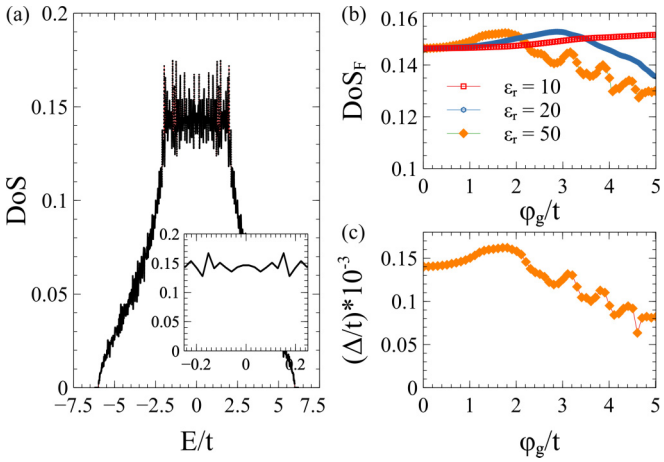

FIG. 6. (a) Density of states versus energy after a smearing with broadening $0.03t$ for a system with $N = 20$ layers and $\epsilon_r = 50$ at zero applied field. Inset: Zoom on a small energy window around the Fermi level at $E = 0$. (b) DoS at the Fermi level as a function of the applied gate voltage for $\epsilon_r = 10, 20, 50$. (c) Gap resulting from solution of Eq. (7) for $\epsilon_r = 50$ and $U = 0.6t$.

VI. TRIANGULAR LATTICE

The results presented show that the behavior of the system is totally due to modification of the DoS induced by the gate voltage, that acts as a confining potential. The effect is more pronounced for systems in which the ratio between the average level spacing and the gap is not too smaller than one. The observations are qualitatively confirmed by changing the in-plane lattice model. It is well known that the square lattice at half filling represents a somewhat peculiar case, with van Hove singularities close to the Fermi level. In Fig. 7(a), we show the results of the simulation for an in-plane triangular lattice. The electric field is screened in few lattice constants,

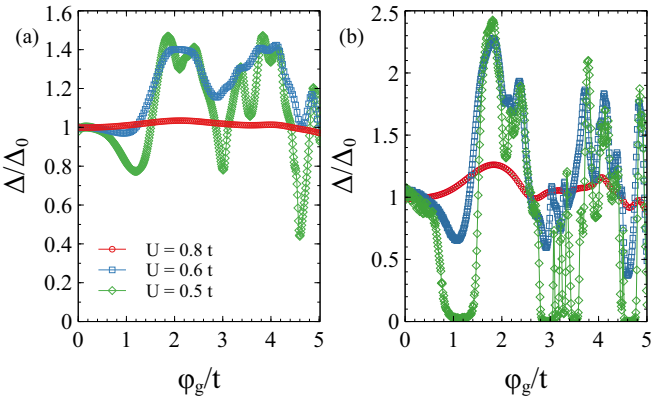

FIG. 7. (a) Gap as a function of the applied gate potential for an in-plane triangular tight-binding model characterized by $N = 20$, $\epsilon_r = 10$, and $N_x = N_y = 100$ for different values of the pairing $U/t = 0.8, 0.6, 0.5$. (b) Same as (a) with the gap is calculated via Eq. (7).

depending on the relative dielectric constant ϵ_r. Contrary to the case of a square lattice, whose spectrum is particle-hole symmetric with respect to the half-filling chemical potential, the triangular lattice shows a different response for positive and negative applied electric field, confirming the expectation that a DoS-mediated mechanism does not produce, in general, an ambipolar effect. Fluctuations of the gap are seen for reduced strengths of the pairing U, confirming the results obtained for the square lattice. The exponential dependence of the gap on the DoS enhances weak variations of the latter when reducing the pairing strength U.

The analysis is repeated by calculating the gap via Eq. (7), with the DoS given by $\nu(E) = \frac{1}{N}\sum_{\mathbf{k}} \delta(E - \epsilon_{\mathbf{k}})$. The spectrum of the slab in the normal state is obtained by including the screened potential, the Hartree shift and the chemical potential at half filling. The result is shown in Fig. 7(b) and qualitatively reproduces the behavior shown in Fig. 7(a) and the general trend according to which a larger gap is less sensitive to the applied electric field. At the same time, we see that a much more pronounced response appears with respect to the one obtained by solving the self-consistent problem. As in the case of the square lattice, an average level spacing of $3 \times 10^{-5}t$ is obtained in energy windows of $0.1t$ around the Fermi energy and the gap at zero applied voltage is $\Delta_0 = 2.9 \times 10^{-4}t$ for $U = 0.6t$, so the gap is just one order of magnitude larger than the average level spacing.

VII. SMALL GRAINS AND DOTS

In the previous sections, we concentrated on studying the behavior of the system for fixed number of points in the BZ. We now study how the system response changes by reducing the number of points in the BZ and study a smaller system that rather describes a clean dot or a grain. By decreasing the size of the system, we expect an enhancement in the sensitivity to the gate that can be due to the increase of average level spacing and overall reduction of DoS. We keep the number of layers to $N = 20$ and reduce the size of the in-plane lattice by setting $N_x = N_y = 80$. The average level spacing has been estimated to be $5.2 \times 10^{-5}t$, which is larger but on the same order than the cases studied in the previous sections. On the other hand, a reduced DoS is observed, with consequent reduction of the gap size at zero gate voltage with respect to the cases analyzed in the previous sections. The average gap Δ versus applied gate is shown in Fig. 8. The curves smoothly decrease to zero, in a fashion similar to the BCS temperature dependence. In Fig. 8(a), we fix $U = 0.5\,t$ and vary the relative dielectric constant ϵ_r. The curves fall all on top of each other upon proper field rescaling (not shown). In Fig. 8(b), we increase the pairing strength and confirm that, for a larger gap, the result remains valid. The behavior is consistent with the nanograin character of the system [25–30], with an average level spacing on order of the zero voltage gap.

To understand the origin of the behavior, we performed analogous simulations for a different in-plane lattice model. For the case of a triangular lattice (results not shown), we notice a strong modulation of the gap with the applied gate voltage, but the smooth decrease to zero is not observed. We then ascribed the behavior shown in Fig. 8 to the peculiar spectrum of the square lattice that features a high degree of nesting of the Fermi surface, with a van Hove singularity appearing at half filling in the infinite in-plane case.

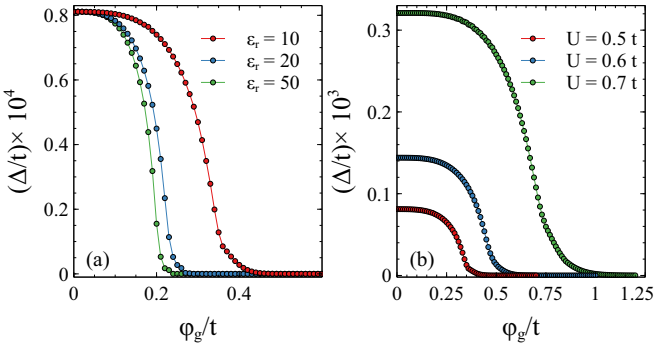

FIG. 8. Gap as a function of the applied gate voltage for a system characterized by $N = 20$ and $N_x = N_y = 80$, with in-plane periodic boundary conditions. (a) $U = 0.5\,t$ varying ϵ_r. (b) $\epsilon_r = 10$ varying U.

VIII. DISCUSSION

The analysis presented tackles the problem of the simultaneous condensation of a superconducting gap and screening of an externally applied field in a fully self-consistent way. The Poisson Eq. (3) includes the part of the Coulomb interaction that describes repulsion of the average charge of each layer and results from minimization of the total energy. It does not include a finite in-plane momentum transfer. The problem is solved exactly at the mean-field level and does not account for phase fluctuations.

The results and methodology open the way to reliable modeling of systems where the surface physics has a nontrivial content, such as the case of a Rashba spin-orbit interaction, that is controlled by an applied electric field, or a multiorbital character of the band structure that enables an electric-field controlled orbital-Rashba effect. Screening in absence of pairing converges very quickly and the joint impact of electric field, sample geometry, and Rashba field can show nontrivial results on the gap.

In summary, we find that in crystalline thin metals, a strong sensitivity to an applied electric field appears in the weak coupling limit, when the gap is just approximately one order of magnitude larger than the average level spacing of the system in the normal state. The latter sets an inverse length scale for the system size, below which the system becomes extremely sensible to applied electric field. In this case, the gap shows sudden rises and falls as the applied voltage is increased that are similar to the well-known shape resonances appearing in the zero temperature gap and in the critical temperature as the thickness of the system is reduced. This behavior reflects the DoS modification induced by the screened potential acting mostly on the outermost few layers. For a perfectly clean crystalline structure, the observed behavior can be understood only in terms of the entire DoS spanning the whole bandwidth. The introduction of an energy smearing in the DoS emulates the effect of disorder and increased thickness, and a moderate broadening washes out the effect, showing a gap that mainly follows the DoS at the Fermi level. Our results are expected to be significant for layered materials and thin crystalline metals

allowing control of superconductivity by an externally applied electrostatic field.

ACKNOWLEDGMENTS

L.C. acknowledges the European Commission for funding through the MSCA Global Fellowship Grant No. TOPOCIRCUS-841894. T.C. acknowledges funding from the European Commission under the Graphene Flagship, Core 3, Grant No. 881603. F.G. acknowledges the EU's Horizon 2020 research and innovation program under Grant Agreement No. 800923 (SUPERTED) and the European Research Council under the EU's Horizon 2020 Grant Agreement No. 899315-TERASEC for partial financial support.

[1] W. Shi, J. Ye, Y. Zhang, R. Suzuki, M. Yoshida, J. Miyazaki, N. Inoue, Y. Saito, and Y. Iwasa, Sci. Rep. **5**, 12534 (2015).
[2] X. Leng, J. Garcia-Barriocanal, B. Yang, Y. Lee, J. Kinney, and A. M. Goldman, Phys. Rev. Lett. **108**, 067004 (2012).
[3] J. Shiogai, Y. Ito, T. Mitsuhashi, T. Nojima, and A. Tsukazaki, Nat. Phys. **12**, 42 (2016).
[4] N. W. Hendrickx, D. P. Franke, A. Sammak, M. Kouwenhoven, D. Sabbagh, L. Yeoh, R. Li, M. L. V. Tagliaferri, M. Virgilio, G. Capellini *et al.*, Nat. Commun. **9**, 2835 (2018).
[5] K. Ueno, S. Nakamura, H. Shimotani, A. Ohtomo, N. Kimura, T. Nojima, H. Aoki, Y. Iwasa, and M. Kawasaki, Nat. Mater. **7**, 855 (2008).
[6] K. Ueno, S. Nakamura, H. Shimotani, H. T. Yuan, N. Kimura, T. Nojima, H. Aoki, Y. Iwasa, and M. Kawasaki, Nat. Nanotechnol. **6**, 408 (2011).
[7] J. T. Ye, Y. J. Zhang, R. Akashi, M. S. Bahramy, R. Arita, and Y. Iwasa, Science **338**, 1193 (2012).
[8] A. D. Caviglia, S. Gariglio, N. Reyren, D. Jaccard, T. Schneider, M. Gabay, S. Thiel, G. Hammerl, J. Mannhart, and J. M. Triscone, Nature (London) **456**, 624 (2008).
[9] Y. Saito, Y. Kasahara, J. Ye, Y. Iwasa, and T. Nojima, Science **350**, 409 (2015).
[10] L. J. Li, E. C. T. O'Farrell, K. P. Loh, G. Eda, B. Özyilmaz, and A. H. Castro Neto, Nature (London) **529**, 185 (2016).
[11] E. Sajadi, T. Palomaki, Z. Fei, W. Zhao, P. Bement, C. Olsen, S. Luescher, X. Xu, J. A. Folk, and D. H. Cobden, Science **362**, 922 (2018).
[12] G. Chen, A. L. Sharpe, P. Gallagher, I. T. Rosen, E. J. Fox, L. Jiang, B. Lyu, H. Li, K. Watanabe, T. Taniguchi *et al.*, Nature (London) **572**, 215 (2019).
[13] A. F. Morpurgo, J. Kong, C. M. Marcus, and H. Dai, Science **286**, 263 (1999).
[14] P. Jarillo-Herrero, J. A. van Dam, and L. P. Kouwenhoven, Nature (London) **439**, 953 (2006).
[15] T. Tsuneta, L. Lechner, and P. J. Hakonen, Phys. Rev. Lett. **98**, 087002 (2007).
[16] A. A. Shanenko and M. D. Croitoru, Phys. Rev. B **73**, 012510 (2006).
[17] A. A. Shanenko, M. D. Croitoru, and F. M. Peeters, Phys. Rev. B **78**, 024505 (2008).
[18] M. D. Croitoru, A. A. Shanenko, C. C. Kaun, and F. M. Peeters, Phys. Rev. B **80**, 024513 (2009).
[19] A. A. Shanenko, M. D. Croitoru, A. Vagov, and F. M. Peeters, Phys. Rev. B **82**, 104524 (2010).
[20] J. M. Blatt and C. J. Thompson, Phys. Rev. Lett. **10**, 332 (1963).
[21] M. Yu, M. Strongin, and A. Paskin, Phys. Rev. B **14**, 996 (1976).
[22] E. H. Hwang, S. Das Sarma, and M. A. Stroscio, Phys. Rev. B **61**, 8659 (2000).
[23] A. A. Shanenko, M. D. Croitoru, and F. M. Peeters, Phys. Rev. B **75**, 014519 (2007).
[24] N. Pinto, S. J. Rezvani, A. Perali, L. Flammia, M. V. Milošević, M. Fretto, C. Cassiago, and N. De Leo, Sci. Rep. **8**, 4710 (2018).
[25] H. Heiselberg, Phys. Rev. A **68**, 053616 (2003).
[26] V. Z. Kresin and Y. N. Ovchinnikov, Phys. Rev. B **74**, 024514 (2006).
[27] A. M. García-García, J. D. Urbina, E. A. Yuzbashyan, K. Richter, and B. L. Altshuler, Phys. Rev. Lett. **100**, 187001 (2008).
[28] S. Bose, A. M. García-García, M. M. Ugeda, J. D. Urbina, C. H. Michaelis, I. Brihuega, and K. Kern, Nat. Mater. **9**, 550 (2010).
[29] M. D. Croitoru, A. A. Shanenko, C. C. Kaun, and F. M. Peeters, Phys. Rev. B **83**, 214509 (2011).
[30] S. Bose and P. Ayyub, Rep. Prog. Phys. **77**, 116503 (2014).
[31] D. Pines. and P. Nozieres, *Theory of Quantum Liquids* (Avalon Publishing, New York, 1999).
[32] N. W. Ashcroft and N. D. Mermin, *Solid State Physics* (Thomson Learning, Toronto, 1976).
[33] G. D. Mahan, *Many-Particle Physics* (Plenum, New York, 2000).
[34] G. F. Giuliani and G. Vignale, *Quantum Theory of the electron liquid* (Cambridge University Press, Cambridge, 2005).
[35] G. De Simoni, F. Paolucci, P. Solinas, E. Strambini, and F. Giazotto, Nat. Nanotechnol. **13**, 802 (2018).
[36] F. Paolucci, G. De Simoni, E. Strambini, P. Solinas, and F. Giazotto, Nano Lett. **18**, 4195 (2018).
[37] F. Paolucci, G. De Simoni, P. Solinas, E. Strambini, N. Ligato, P. Virtanen, A. Braggio, and F. Giazotto, Phys. Rev. Appl. **11**, 024061 (2019).
[38] F. Paolucci, G. De Simoni, P. Solinas, E. Strambini, C. Puglia, N. Ligato, and F. Giazotto, AVS Quantum Sci. **1**, 016501 (2019).
[39] G. De Simoni, C. Puglia, and F. Giazotto, Appl. Phys. Lett. **116**, 242601 (2020).
[40] G. De Simoni, F. Paolucci, C. Puglia, and F. Giazotto, ACS Nano **13**, 7871 (2019).
[41] L. Bours, M. T. Mercaldo, M. Cuoco, E. Strambini, and F. Giazotto, Phys. Rev. Res. **2**, 033353 (2020).
[42] I. Golokolenov, A. Guthrie, S. Kafanov, Y. Pashkin, and V. Tsepelin, arXiv:2009.00683.
[43] L. D. Alegria, C. G. Bøttcher, A. K. Saydjari, A. T. Pierce, S. H. Lee, S. P. Harvey, U. Vool, and A. Yacoby, Nat. Nanotechnol. **16**, 404 (2021).
[44] M. F. Ritter, A. Fuhrer, D. Z. Haxell, S. Hart, P. Gumann, H. Riel, and F. Nichele, Nat. Comm. **12**, 1266 (2021).
[45] M. Rocci, G. De Simoni, C. Puglia, D. D. Esposti, E. Strambini, V. Zannier, L. Sorba, and F. Giazotto, ACS Nano **14**, 12621 (2020).

[46] C. Puglia, G. De Simoni, and F. Giazotto, Phys. Rev. Appl. **13**, 054026 (2020).
[47] M. T. Mercaldo, P. Solinas, F. Giazotto, and M. Cuoco, Phys. Rev. Appl. **14**, 034041 (2020).
[48] Y. Fukaya, K. Yada, Y. Tanaka, P. Gentile, and M. Cuoco, Phys. Rev. B **102**, 144512 (2020).
[49] P. Solinas, A. Amoretti, and F. Giazotto, Phys. Rev. Lett. **126**, 117001 (2021).
[50] P. W. Anderson, Phys. Rev. **112**, 1900 (1958).
[51] D. J. Thouless, Ann. Phys. **10**, 553 (1960).
[52] P. Virtanen, A. Braggio, and F. Giazotto, Phys. Rev. B **100**, 224506 (2019).